Optical Fiber Technology 74 (2022) 103077

Contents lists available at ScienceDirect

Optical Fiber Technology

journal homepage: www.elsevier.com/locate/yofte

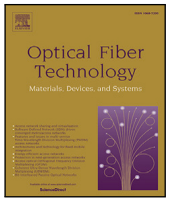

Assessing the quality of transmission of lightpaths in multiband C+L networks through Gaussian noise models

Pedro Venda [a], João Rebola [a,b,*], Luís Cancela [a,b]

[a] Iscte - Instituto Universitário de Lisboa, Lisbon, Portugal
[b] Optical Communications and Photonics Group, Instituto de Telecomunicações, Lisbon, Portugal

ARTICLE INFO

Keywords:
Gaussian noise
Multiband transmission
Nonlinear interference
Optical networks
Stimulated Raman scattering

ABSTRACT

In an optical network scenario, wavelength division-multiplexing (WDM) channels are constantly being added and dropped, leading to dynamic traffic variations in the lightpaths. In this work, the impact of the network traffic load and spectral occupancy on the quality of transmission, namely on the normalized nonlinear interference (NLI) power, power transfer due to stimulated Raman scattering (SRS) and optical signal-to-noise ratio (OSNR) of the lightpaths in a C+L multiband optical network is assessed using the recently proposed closed-form interchannel SRS Gaussian noise model (ISRS GN-model). We show that, due to the dynamic traffic behavior, the normalized NLI power can oscillate up to 2 dB in the highest frequency channels due to NLI variations when the tested channels have unequal spacing along the spectrum. For the optimum channel launch power and by increasing the network traffic load, the power transfer between the outer channels can increase up to 5.1 dB due to the SRS effect. With 201 WDM channels, high traffic load and for the optimum channel power, we obtained a maximum OSNR variation along the channel frequencies of only about 0.7 dB. A comparison between the OSNR predictions of the closed-form ISRS GN-model and a closed-form Gaussian noise (GN) model that does not take into account the SRS effect is also performed. In all results obtained, the maximum difference between the OSNR predictions of GN (without SRS) and ISRS GN models is below 0.7 dB at optimum OSNR and maximum C+L band occupancy. For channel launch powers higher than the optimum, the OSNR differences increase up to 3 dB.

1. Introduction

Nowadays, the C-band, comprising approximately 4.8 THz bandwidth, is typically used for transmission in single mode optical fibers (SMFs). Recently, there has been a tremendous effort in using this bandwidth resource in the most efficient way [1]. Bandwidth-variable transponders, adaptive bit rate/modulation formats and flexible grid, yielded more dynamism to the wavelength-division multiplexing (WDM) channels assignment in optical networks and enabled to maximize the utilization of the spectrum in the C-band [2,3].

However, it is widely accepted that the transport capacity of today's optical networks, using the C-band only [4], will not be capable of carrying the amount of data traffic expected in the coming years [5]. The use of additional bands of the widely deployed low-loss spectrum of Zero Water Peak SMFs (ITU-T G652.D), i.e., the multiband solution, is seen as a promising approach to increase the transmission bandwidth, avoiding the costly investments required by space-division multiplexing solutions [6]. In theory, a multiband solution can achieve up to 8 times capacity increase, if the complete 48 THz bandwidth is exploited. Currently, the first generation of multiband solutions, which augments capacity via exploiting also the L-band (i.e., C+L-band transmission), allows to increase the available bandwidth to almost 10 THz and has already been deployed in a small number of long-haul terrestrial networks [7].

The transmission of WDM channels in multiband solutions is highly impacted by the stimulated Raman scattering (SRS) effect. Therefore, the impact of SRS must be properly modeled to accurately evaluate the quality of transmission (QoT) of each network lightpath. In optical networks, QoT evaluation resorting to the split-step Fourier method is unfeasible (has been only performed for validation purposes [8]) and lightpaths QoT is usually assessed using the generalized optical signal-to-noise ratio (OSNR) and by estimating the nonlinear interference (NLI) using the Gaussian noise (GN) model [9]. A GN model for multiband networks QoT evaluation was proposed in [8], (interchannel SRS (ISRS)-GN model), and in [10,11] (generalized GN (GGN)-model) and its accuracy experimentally verified in [9,12]. However, such models are outside the computation time frame required by network analysis

* Corresponding author.
E-mail address: joao.rebola@iscte-iul.pt (J. Rebola).

https://doi.org/10.1016/j.yofte.2022.103077
Received 5 June 2022; Received in revised form 31 August 2022; Accepted 24 September 2022
Available online 22 October 2022
1068-5200/© 2022 The Authors. Published by Elsevier Inc. This is an open access article under the CC BY-NC-ND license (http://creativecommons.org/licenses/by-nc-nd/4.0/).

and optimization because they require numerically solving multiple integrals to obtain the NLI and solving Raman equations to accurately describe the SRS. In [13], an accurate model based on closed-form expressions for assessing the QoT accounting for NLI and SRS interaction has been proposed.

Multiband network performance and optimization studies using the closed-form ISRS GN-model have been performed in [2,14–16]. In [2], the QoT of the network lightpaths is assessed considering the worst-case of full C+L band spectral occupancy, when it is known that the QoT estimation based on the present state of spectral occupancy can provide a data capacity gain to the network. The latter works are more focused on demonstrating the network gains, by optimizing the network with the present state of spectral occupancy [14,15] or on following a network upgrading strategy based on QoT estimation [16]. All these works [2,14–16] are more focused on network analysis and optimization and such analyses may conceal the effect of varying several system parameters, such as dynamic traffic variations, spectral occupancy, channels launch power, on more physical QoT related quantities, such as NLI power, OSNR and power transfer due to SRS. Only in [13], a preliminary study of the effect of the dynamic traffic variations on the NLI considering full spectral occupancy was performed for validation purposes, without assessing its impact on the OSNR.

In this work, an exhaustive analysis of several WDM system parameters, such as dynamic traffic variations, number of channels under test, launch power, channels spacing, C+L band spectral occupancy and channel distribution along the WDM spectrum is carried out in order to assess their impact on SRS, NLI power and OSNR at the end of a network lightpath, using the closed-form ISRS GN-model introduced in [13]. Additionally, the accuracy of the closed-form GN-model proposed in [17] valid only for C-band network transmission is compared with the closed-form ISRS GN-model proposed for multiband transmission, which to the best of our knowledge has not been done yet. From this comparison, we show that the closed-form GN-model proposed in [17] can also be applied to assess the performance in multiband C+L networks without much loss of accuracy, if the system is set up to operate at the optimum launch power level.

This paper is organized as follows. In Section 2, the main definitions and assumptions used for simulating the network lightpaths and assess their performance are presented and explained. In Section 3, the impact of the network traffic load, number of channels under test and launch power on NLI, power transfer due to SRS and OSNR of a lightpath is quantified. In Section 4, the comparison between the two closed-form GN models regarding the network lightpaths performance estimation is performed. Section 5 presents the conclusions.

2. Model for assessing the lightpaths QoT

In this section, the definitions and assumptions considered in this work to simulate dynamic traffic variations and spectral occupancy in the network lightpaths are presented and explained.

The two lightpaths examples studied in this work, taken from the British Telecommunications network topology [13], are illustrated in Fig. 1. The ROADMs architecture considered is the route-and-select with maximum losses of 18 dB [18]. The filtering effects and crosstalk due to ROADM components imperfections [19] are not taken into account in this work. The post-amplifiers are designed to perfectly compensate the ROADM maximum losses. The inline and pre-amplifiers compensate perfectly the previous fiber losses. All optical amplifiers considered in the lightpaths are erbium doped fiber amplifiers (EDFAs) with dynamic gain equalization, performed using ideal gain-flattening filters [8]. Thus, at the output of each EDFA, the power transfer due to SRS is compensated. The OSNR is estimated at the end of the lightpath before the optical receiver, as highlighted in Fig. 1.

For the analysis of the lightpaths of Fig. 1, the WDM wavelengths are classified in two categories: channels under test (CUTs) and add/drop channels. The CUTs correspond to the WDM channels that are

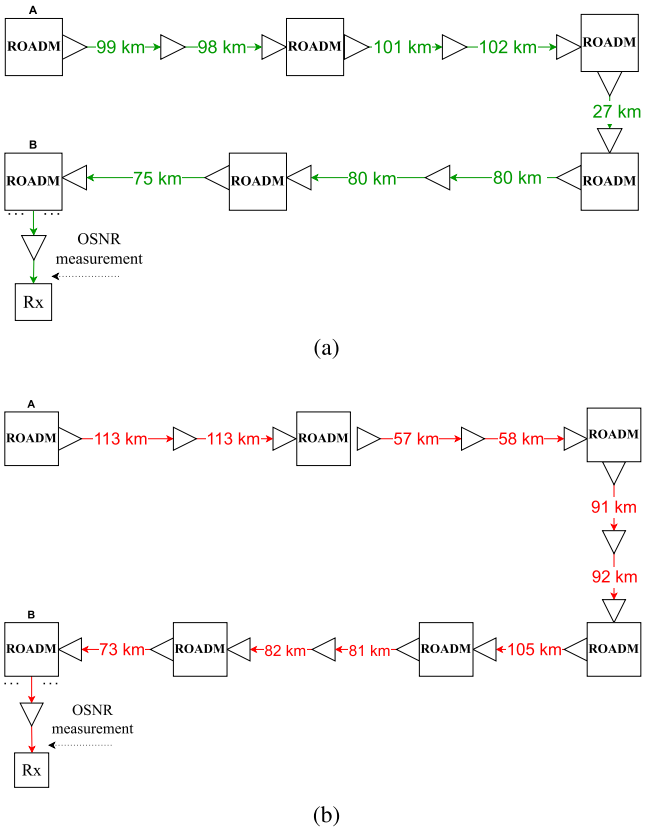

Fig. 1. Two lightpaths examples taken from the British Telecommunications topology of the United Kingdom core network [13,20]. Throughout this work, the lightpaths in (a) and (b) are referred to as green and red lightpaths, respectively.

transmitted/expressed along the complete lightpath, i.e., from the first node to the last node without any add/drop occurring in those wavelengths. The add/drop channels are the wavelengths that can be added or dropped in any ROADM of the considered lightpath.

The two following definitions are introduced: *network utilization* and *C+L band occupancy*. For a given span of a lightpath, the ratio between the number of channels transmitted in the j-th span and the total number of channels is defined as span utilization, which is denoted as $\epsilon_{\text{span},j}$. For the entire lightpath, the network utilization $\epsilon_{\text{network}}$ is defined as the average of the network utilizations of all spans, written as

$$\epsilon_{\text{network}} = \frac{1}{N_s}\sum_{j=1}^{N_s}\epsilon_{\text{span},j} = \frac{1}{N_s}\sum_{j=1}^{N_s}\frac{N_{ch,j}}{N_{ch}} \tag{1}$$

where $N_{ch,j}$ is the number of channels transmitted in the j-th span, N_s is the number of spans in the lightpath and N_{ch} is the total number of WDM channels considered. The C+L band occupancy $\epsilon_{\text{occupancy}}$ is defined as

$$\epsilon_{\text{occupancy}} = \frac{\Delta f \cdot N_{ch}}{B_{\text{C+L-band}}} \tag{2}$$

where Δf is the channel spacing and $B_{\text{C+L-band}}$ is the total C+L optical transmission bandwidth, assumed as 11.5 THz [21], corresponding to 100% C+L band occupancy.

In each ROADM, the add/drop channels are added or dropped randomly considering a uniform distribution to emulate the behavior of dynamic traffic load variations occurring at the ROADM nodes [13,15]. Although the add/drop operations do not follow a uniform distribution in a real dynamic network, this simplified assumption allowed us to study the effect of dynamic traffic variations on the OSNR and on the accuracy of the closed-form expressions, as we intended. The number of add/drop channels depends on the required $\epsilon_{\text{network}}$. The launch power

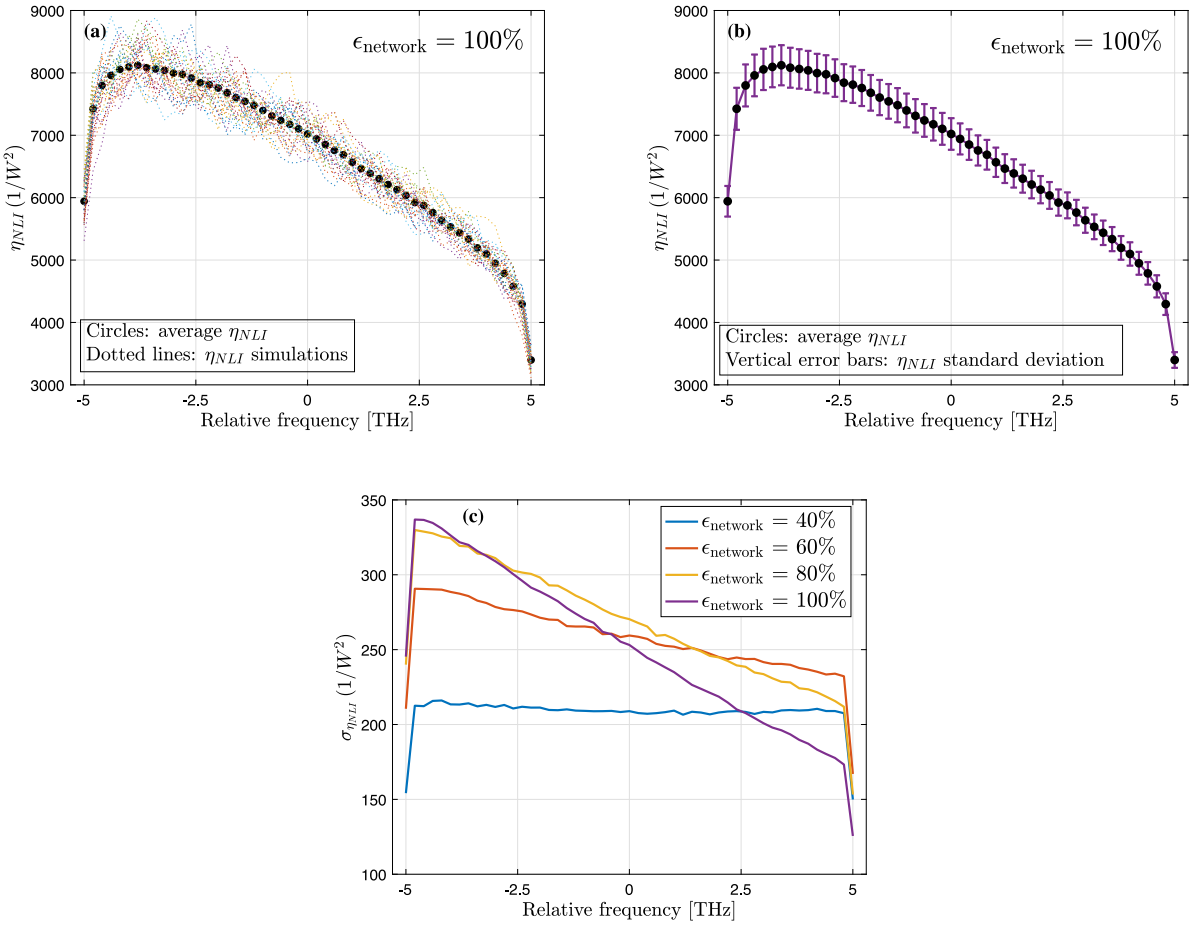

Fig. 2. In (a), several simulated realizations of η_{NLI} and its average are shown as a function of CUTs frequency, for $\epsilon_{\text{network}} = 100\%$. Considering the same network utilization, in (b), the average η_{NLI} and corresponding standard deviation $\sigma_{\eta_{NLI}}$ are depicted. In (c), the standard deviation $\sigma_{\eta_{NLI}}$ is shown as a function of CUTs frequency, for network utilizations of 40%, 60%, 80% and 100%.

of the added channels has a random offset of ±1 dB in relation to the launch power of the CUTs. For a more realistic approach, the added channels always maintain the same launch power along their lightpath until they are dropped, i.e., along the lightpaths shown in Fig. 1, the launch power of a channel only changes if it is added to the optical network more than one time. This last assumption differs from the optical transmission scenario considered in [13], where the add/drop channels that have not been dropped may not maintain, at each span input, the launch power they had in the previous span. The launch powers of the CUTs remain the same along the complete lightpath.

All NLI contributions along an optical link composed by several fiber spans sum coherently or incoherently along the signal propagation until the receiver [22]. Along this work, the coherent and incoherent variants of the ISRS GN-model will be referred to as the coherent ISRS GN-model and incoherent ISRS GN-model, respectively. Due to the asymptotic expansion of the dilog function performed in its derivation, we will refer to the SRS-unaware GN-model as the asymptotic GN-model [17]. This model considers that the NLI accumulates incoherently. It should be noted that among the GN models covered, the coherent ISRS GN-model is the one that provides NLI estimation results closest to the split-step Fourier method [13], and therefore, it is the more accurate model to estimate the OSNR.

The mathematical expressions concerning the calculation of the NLI power and OSNR using the closed formulas of the GN-model have been implemented in the Matlab software on a computer with 16 GB RAM and Intel Core i7-6700K 4 GHz processor. The red and green lightpaths are characterized by the distances shown in Fig. 1 and fiber parameters, gains and noise figures of the EDFAs. To emulate the network environment and the dynamic traffic variations, a matrix corresponding to the powers of the WDM channels at the input of each fiber span is generated in each simulation realization, according to the assumptions already described.

Table 1
System parameters for Section 3.1.

System parameters	
Number of channels (N_{ch})	251
Channel spacing (Δf) [GHz]	40
Symbol rate (R_s) [GBaud]	40
Channel bandwidth (B_m) [GHz]	40
Loss coefficient (α) [dB/km]	0.2
Dispersion (β_2) [ps/nm/km]	17
Dispersion slope (S_r) [ps/nm^2/km]	0.067
NLI coefficient (γ) [W^{-1}km^{-1}]	1.2
Raman gain slope (C_r) [W^{-1}km^{-1}THz^{-1}]	0.028

Using the system parameters shown in Table 1, the performance assessment of the network lightpaths used in this work has been successfully validated according to the normalized NLI power results shown in Fig. 8 of [13].

3. Impact of WDM system parameters variation on NLI and OSNR predictions

In this section, the aim is to analyze how several network parameters, with a special emphasis on the network utilization $\epsilon_{\text{network}}$, impact the normalized NLI power η_{NLI} and OSNR estimation using the ISRS GN-model. Only the coherent ISRS GN-model is used in this section.

3.1. Impact of network utilization, number of channels under test and their spectral distribution on NLI prediction

One of the consequences of the dynamic variations of the add/drop channels in the fiber spans is the oscillatory behavior of the NLI prediction, each time a lightpath has a given network utilization [13]. In Fig. 2(a), the CUTs average normalized NLI power and some simulated dynamic traffic load realizations are represented as a function of the WDM signal frequency, for $\epsilon_{\text{network}} = 100\%$. In Fig. 2(b), the standard deviation of the normalized NLI power $\sigma_{\eta_{NLI}}$ is also represented through the error bars. The standard deviation $\sigma_{\eta_{NLI}}$ of the CUTs is shown in Fig. 2(c) as a function of their center frequencies, for different network utilizations. In order to obtain stabilized average NLI predictions over the entire WDM spectrum, 200 simulations are performed. To calculate each corresponding standard deviation, 30,000 simulations are considered. By simulation, we mean one calculation of the normalized NLI power η_{NLI} using Eq. (5) of [13] with a given network utilization. Table 1 shows the system parameters considered for this study.

Fig. 2 shows that, in general, the standard deviation $\sigma_{\eta_{NLI}}$ increases as the WDM signal frequency decreases, meaning that there is a greater oscillatory behavior of η_{NLI} in the lower frequency channels, when compared with higher frequency channels. By analyzing Fig. 2(a) for $\epsilon_{\text{network}} = 100\%$, it can be seen that, with the exception of the edge channels, the η_{NLI} estimates are more dispersed around their average in the lower frequency components. This can be confirmed by the higher $\sigma_{\eta_{NLI}}$ found in these frequencies, illustrated through the error bars in Fig. 2(b). As $\epsilon_{\text{network}}$ decreases, the difference between the standard deviation $\sigma_{\eta_{NLI}}$ of the higher and lower frequencies is also reduced, as can be seen in Fig. 2(c).

In Fig. 3(a), the CUTs average normalized NLI power η_{NLI} is represented as a function of the WDM channels frequency, for the network utilizations: 20%, 60% and 100%. In Fig. 3(b), the power transfer between the outer channels $\Delta\rho(L)$, as defined in [8], is depicted as a function of the network utilization, for several CUTs launch powers. The power transfer $\Delta\rho(L)$ is calculated by averaging the power transfers obtained in all spans of the lightpaths. The number of CUTs considered, $N_{CUT} = 51$, is approximately 20% of the total number of WDM channels.

The average η_{NLI} exhibits a stable behavior after 200 simulations for the three network utilizations considered, as can be seen in Fig. 3(a). As the network utilization increases, the number of transmitted WDM channels grows, thus increasing the NLI magnitude and the tilt of its variation across the WDM signal. Due to the additional two spans, the red lightpath is more impacted by the NLI than the green lightpath, with a constant η_{NLI} power difference of 1 dB for the entire signal bandwidth.

From Fig. 3(b), the η_{NLI} increase with the network utilization is explained through the higher power transfer $\Delta\rho(L)$ between the outer channels as $\epsilon_{\text{network}}$ grows. This figure also shows that $\Delta\rho(L)$ varies more sharply as the CUTs launch power P_{CUT} increases due to the highest impact of SRS. For $P_{\text{CUT}} = 5$ dBm, there is a power transfer increase of about 16.4 dB from $\epsilon_{\text{network}} = 20\%$ to $\epsilon_{\text{network}} = 100\%$, whereas for $P_{\text{CUT}} = 0$ dBm, the power transfer increases about 5.1 dB.

Fig. 4 shows the normalized NLI power η_{NLI} as a function of the WDM signal frequency, for $N_{CUT} = 10\%N_{ch}$, $N_{CUT} = 50\%N_{ch}$ and $N_{CUT} = N_{ch}$, network utilizations of 50%, 70% and 100% and the red lightpath. The average value of η_{NLI} is obtained after 200 simulations of dynamic traffic. As in the previous study, in Fig. 4(a), the CUTs are placed equidistant in frequency over the entire WDM signal bandwidth. The crosses represent the results when the CUTs corresponding to 10% of the total number of channels are located only on the left side of the spectrum. In Fig. 4(b), a random unequal spacing of the CUTs is considered. The launch power of the CUTs is 0 dBm.

Fig. 4(a) shows that as the number of CUTs is reduced, there is an increase of η_{NLI} across the entire WDM signal bandwidth, which

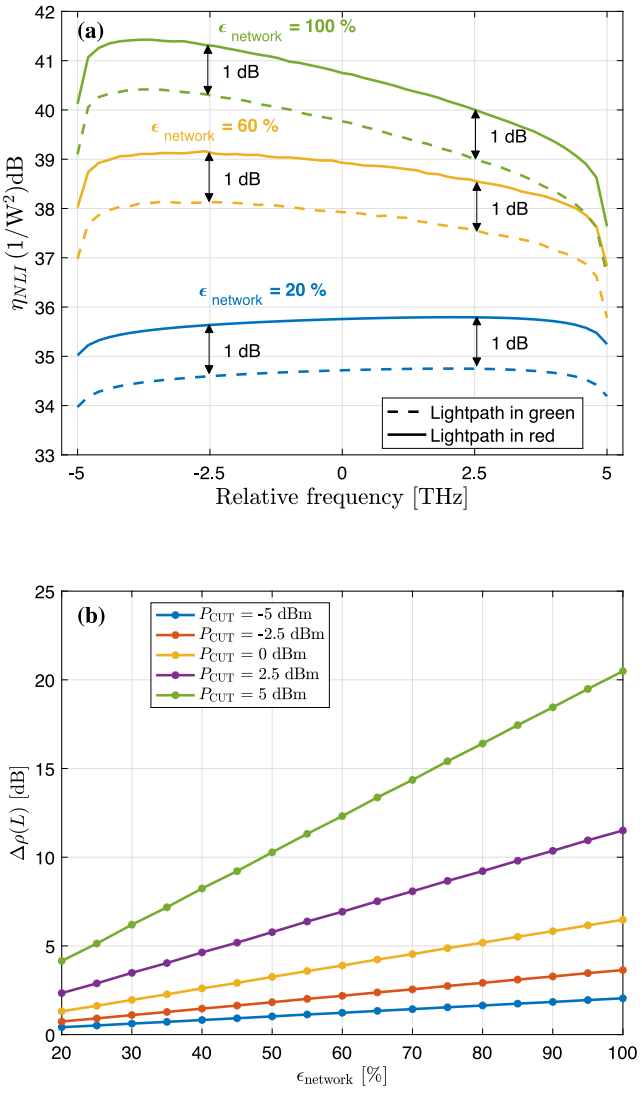

Fig. 3. In (a), the variation of the average η_{NLI} with the WDM signal frequency is depicted, for $P_{CUT} = 0$ dBm and network utilizations of 20%, 60% and 100%. In (b), the power transfer $\Delta\rho(L)$ is represented as a function of the network utilization, for the red lightpath. The number of CUTs is 20% of the number of WDM channels and the C+L band occupancy is 87%.

is more pronounced for low network utilizations. For $\epsilon_{\text{network}} = 50\%$, the normalized NLI power difference is about 0.3 dB between the cases of $N_{\text{CUT}} = 10\%N_{ch}$ and $50\%N_{ch}$. For $\epsilon_{\text{network}} = 70\%$, this difference is below 0.2 dB. For $\epsilon_{\text{network}} = 100\%$, the maximum difference is only 0.1 dB between $N_{\text{CUT}} = 10\%N_{ch}$ and $N_{\text{CUT}} = N_{ch}$. The NLI is higher when the CUTs are only on the left side of the spectrum, due to the enhanced interference between channels as the CUTs are closer in frequency.

In Fig. 4(b), with an unequal CUTs spacing (channels randomly positioned along the spectrum), the normalized NLI power shows a considerable fluctuating behavior for $\epsilon_{\text{network}} < 100\%$. The highest η_{NLI} oscillation behavior occurs when $N_{\text{CUT}} = 50\% \cdot N_{ch}$ and $\epsilon_{\text{network}} = 50\%$, reaching maximum oscillations of about 2 dB between the highest frequency channels. Very negligible oscillations occur when $\epsilon_{\text{network}} = 100\%$, independently of the number of CUTs considered. For $\epsilon_{\text{network}} = 100\%$, $N_{\text{CUT}} = N_{ch}$, there are no add/drop channels and, so, it is insignificant how the CUTs are spaced in frequency.

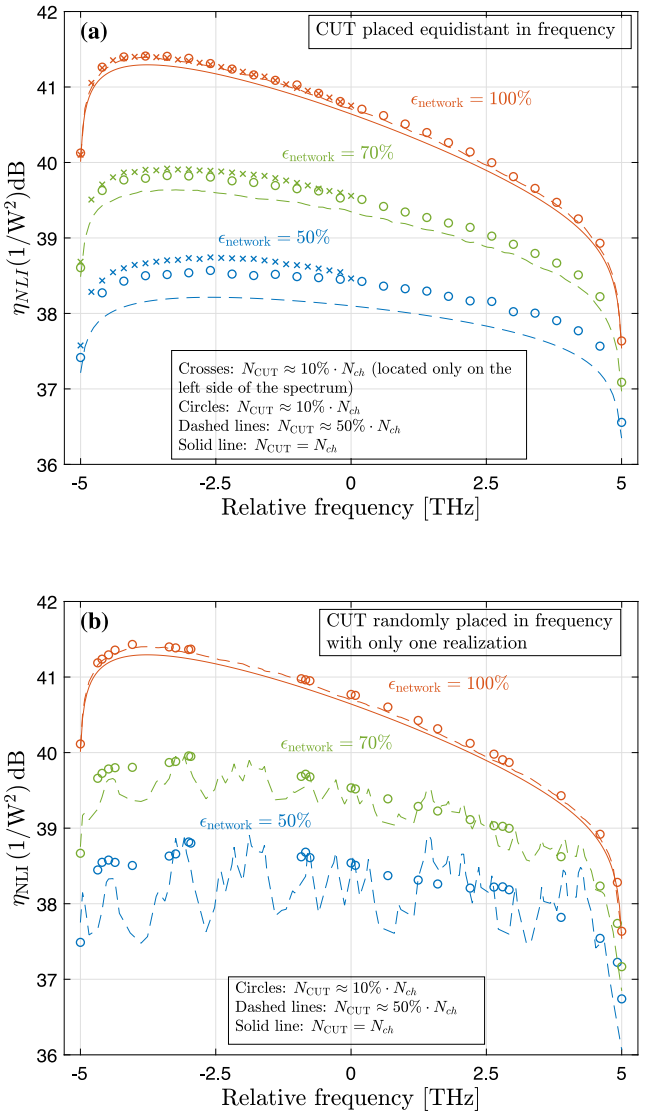

Fig. 4. Average η_{NLI} of the CUTs as a function of frequency, for $\epsilon_{\text{occupancy}} = 87\%$, several number of channels under test and network utilizations. In (a), the CUTs are placed equidistant in frequency. In (b), the CUTs are randomly positioned with an unequal frequency spacing along the WDM spectrum. Only the red lightpath is considered.

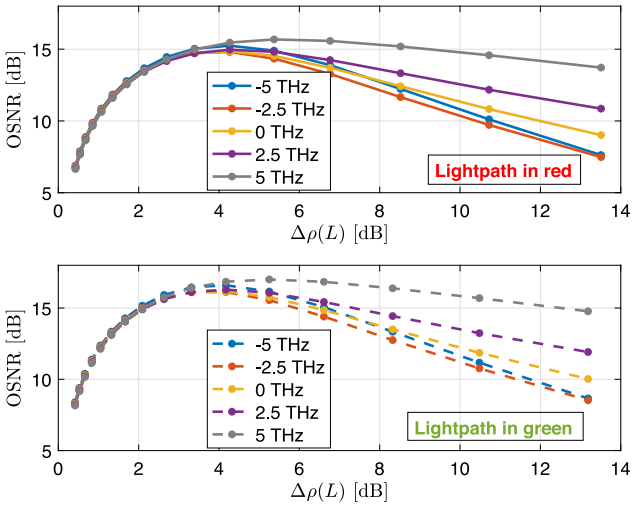

Fig. 5. OSNR as a function of the power transfer between the outer channels $\Delta\rho(L)$, for $\epsilon_{\text{occupancy}} = 87\%$, $\epsilon_{\text{network}} = 90\%$, $N_{CUT} = 20\% \cdot N_{ch}$ and the red and green lightpaths.

Table 2
System parameters for Sections 4 and 3.2.

System parameters	
Number of channels (N_{ch})	201
Number of channels under test (N_{CUT})	41
Channel spacing (Δf) [GHz]	50
Symbol rate (R_s) [GBaud]	32
Channel bandwidth (B_m) [GHz]	32
Loss coefficient (α) [dB/km]	0.22
Dispersion (β_2) [ps/nm/km]	16.7
Dispersion slope (S_r) [ps/nm^2/km]	0.067
NLI coefficient (γ) [W^{-1}km^{-1}]	1.3
Raman gain slope (C_r) [W^{-1}km^{-1}THz^{-1}]	0.028
Noise figure (F_n) [dB]	5

3.2. Network utilization impact on OSNR

In this subsection, the impact of the network utilization on the OSNR estimation using the ISRS GN-model is evaluated. The system parameters considered for the OSNR calculation are presented in Table 2. In this work, we assume that the impact of the SRS on the ASE noise power is negligible.

In Fig. 5, the OSNR is depicted as a function of the power transfer between the outer channels, for $\epsilon_{\text{occupancy}} = 87\%$, $\epsilon_{\text{network}} = 90\%$ and for the channels allocated in the frequencies: −5, −2.5, 0, 2.5 and 5 THz. To increase the power transfer $\Delta\rho(L)$, the launch power of the CUTs is increased.

The OSNR starts to grow with the increase of the power transfer, reaching the maximum between $\Delta\rho(L) \approx 3.5$ dB and 6 dB, for both lightpaths and depending on the channel frequency. After reaching the maximum value, the OSNR decreases more smoothly for all signal frequencies, practically with a linear behavior. As the channel power increases, for lower power transfers, the OSNR increases, since the amplifiers noise is the dominant contribution to the performance degradation. By further increasing the launch power, the NLI starts to have a significant contribution to the performance degradation, the OSNR variation is smoothed and reaches the maximum value. After this maximum, the NLI becomes dominant and starts to degrade the system performance, leading to the decreasing OSNR observed in Fig. 5. For the center channel, the CUTs launch power of approximately 0 dBm leads to the power transfer of around 4 dB that allows obtaining the maximum OSNR of about 14.9 dB and 16.2 dB, for the red and green lightpaths, respectively. For this optimum power, i.e., when the OSNR maximum is reached in Fig. 5, the maximum OSNR variation between the five WDM channels is only about 0.7 dB.

The OSNR as a function of the CUTs frequencies is shown in Figs. 6(a) and 6(b), for $\epsilon_{\text{occupancy}} = 87\%$ and $\epsilon_{\text{network}} = 30\%$, 50%, 70% and 90%, for the CUTs launch power, respectively, of 0 dBm and 5 dBm. In Fig. 6(a), the power transfers of the green and red lightpaths are, respectively, about 4.2 dB and 4.3 dB and, in Fig. 6(b), about 13.2 dB and 13.5 dB. Notice that, according to Fig. 5, for $\epsilon_{\text{network}} = 90\%$, a power transfer of about 4 dB corresponds to a OSNR very close to the maximum and a power transfer of about 13 dB leads to a significantly lower OSNR due to the increased impact of the joint effect of NLI and SRS.

In general, Fig. 6 shows that the OSNR decreases as the network utilization grows. This is a consequence of the increase of the NLI power with the network utilization, as shown in Fig. 3(a). Also as an effect of the increase of the NLI power, it can be seen that as the network utilization increases, the OSNR variation tends to tilt, with the higher frequency components of the WDM signal performing better than the lower frequency components. Due to the high power transfer used in Fig. 6(b), the OSNR tilt is much more sharper than in Fig. 6(a), which

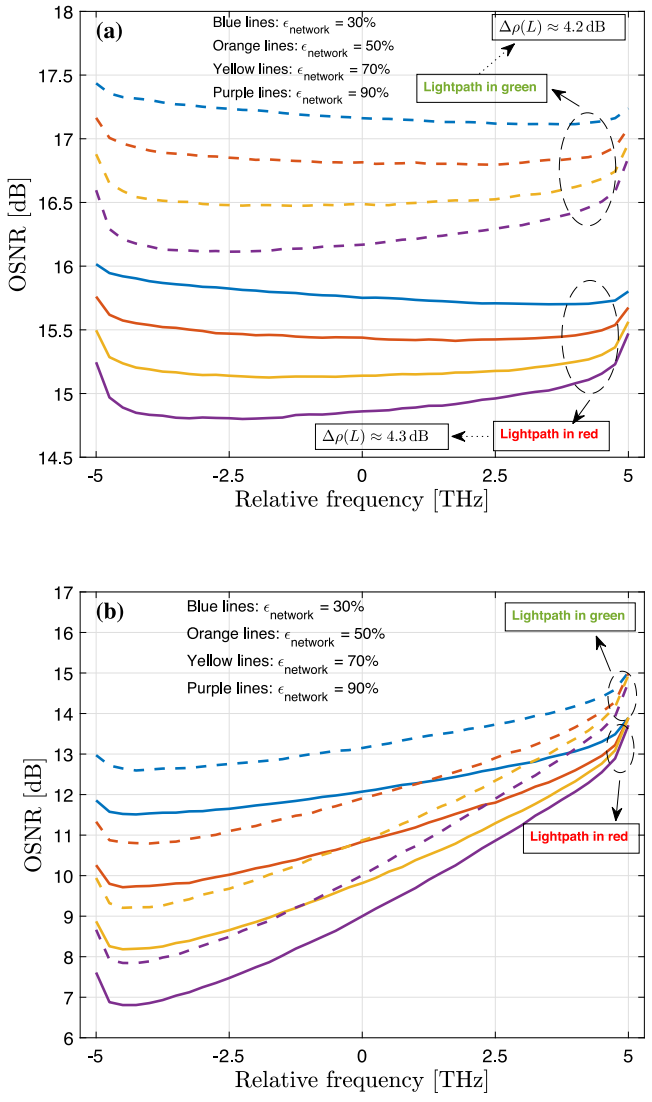

Fig. 6. OSNR as a function of the frequency, for $\epsilon_{\text{occupancy}} = 87\%$, $N_{CUT} = 20\% \cdot N_{ch}$ and network utilizations of 30%, 50%, 70% and 90%. The CUTs launch power considered is 0 dBm in (a) and 5 dBm in (b). The lightpaths used are illustrated in Fig. 1.

means that the lowest frequency channels are much more impacted by NLI. For instance, in Fig. 6(a), there is an OSNR difference of only about 0.5 dB between the outer channels for $\epsilon_{\text{network}} = 90\%$, whereas in Fig. 6(b), this difference rises to about 6 dB.

4. GN models comparison

In the following, the OSNR obtained using the ISRS GN-model is compared with the OSNR given by the asymptotic GN-model designed only for the C-band [17, Eq. (16)]. The variation of the OSNR with the C+L band occupancy is also analyzed.

4.1. OSNR over the C+L band at optimum launch power

The OSNR and power transfer $\Delta\rho(L)$ for the red and green lightpaths as a function of the C+L band occupancy are shown in Fig. 7(a) for the WDM lowest frequency channel, in Fig. 7(b) for the center channel and in Fig. 7(c) for the highest frequency channel. The network utilization considered is about 95%. The CUTs power is set to $P_{CUT} = 0$ dBm. For the C+L band WDM system studied, this power leads to approximately the maximum OSNR along the several WDM channels, as shown in

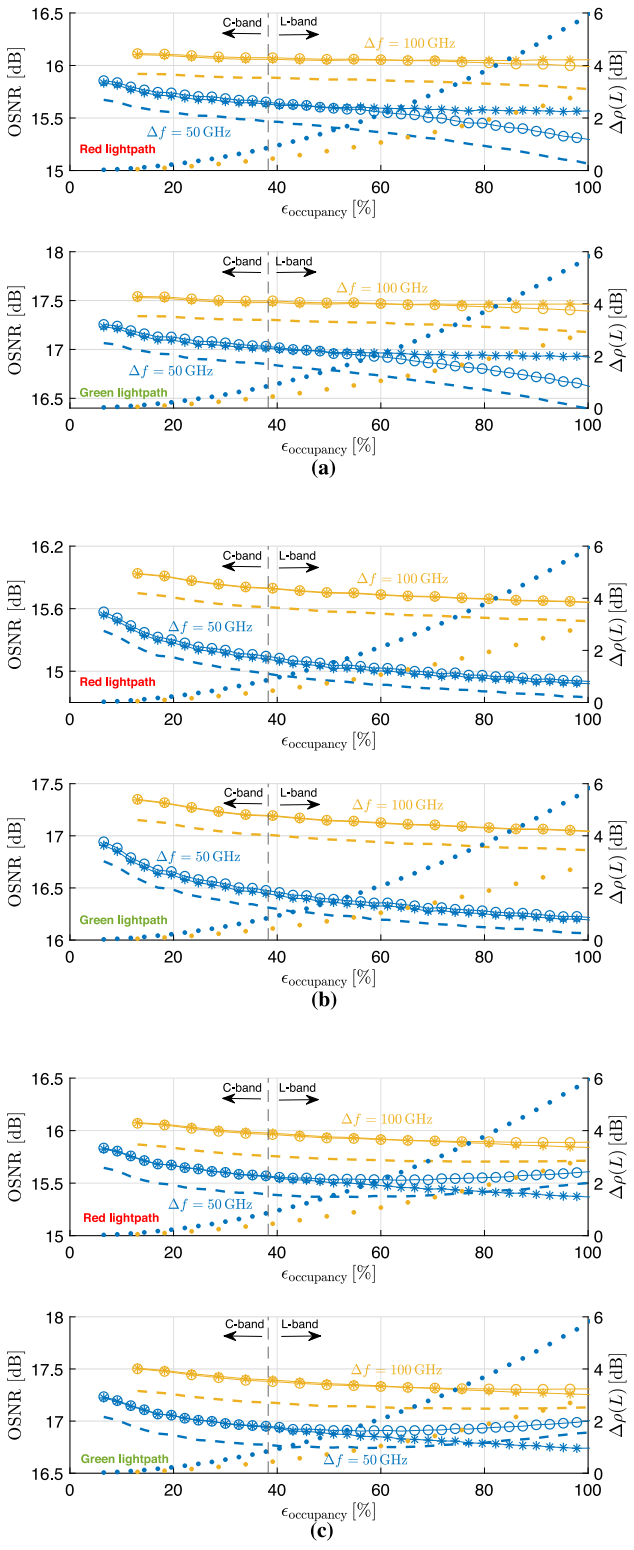

Fig. 7. OSNR as a function of the C+L band occupancy, for the center channel in (b) and the lowest and highest WDM channels in (a) and (c), respectively. The network utilization is 95% and $N_{CUT} = 20\% \cdot N_{ch}$. Circles: closed-form ISRS GN-model (incoherent). Dashed lines: closed-form ISRS GN-model (coherent). Asterisks: asymptotic GN-model. Points: $\Delta\rho(L)$.

Fig. 5. The lowest, center and highest frequency channels are always assumed to be CUTs. Using a uniform distribution, the remaining CUTs

are chosen randomly until 20% of the available WDM channels are occupied, i.e., $N_{CUT} = 20\% N_{ch}$. Two channels spacings are considered: 50 GHz (blue lines) and 100 GHz (yellow lines). To increase the C+L band occupancy, the channels are added sequentially in the total available bandwidth, i.e., first, the C-band is filled and then the L-band. The division that marks the end of the C-band and the beginning of the L-band is highlighted by the dashed black vertical lines in Fig. 7.

In Fig. 7(b), for the center channel and the two channel spacings, the OSNR predictions using the asymptotic GN-model show a very good agreement with the ones obtained with the incoherent ISRS GN-model for all values of the C+L band occupancy. Due to higher NLI predictions, the coherent ISRS GN-model provides lower OSNRs in the center channel, with a 0.2 dB maximum difference in relation to the other two GN models.

For $\Delta f = 50$ GHz and $\epsilon_{\text{occupancy}}$ above around 70%, the asymptotic GN-model overestimates and underestimates the OSNR for the lowest and highest WDM frequencies, respectively, in relation to the incoherent ISRS GN-model results. The maximum OSNR difference of 0.3 dB between these two models is reached when the C+L band is completely filled and the average power transfer is approximately 6 dB. The maximum OSNR discrepancy between the asymptotic GN-model and the coherent ISRS GN-model is about 0.5 dB and is reached for $\Delta f = 50$ GHz and $\epsilon_{\text{occupancy}} = 100\%$. These higher OSNR discrepancies encountered for $\Delta f = 50$ GHz are due to the higher SRS power transfer in relation to the power transfer obtained for the 100 GHz channel spacing. The OSNR differences between the GN models are approximately the same for both lightpaths considered.

4.2. OSNR considering different CUTs launch powers

In Fig. 8, the OSNR is depicted as a function of the CUTs frequencies, for (a) $P_{CUT} = -3$ dBm, (b) $P_{CUT} = 0$ dBm and (c) $P_{CUT} = 3$ dBm, for $\epsilon_{\text{occupancy}} = 100\%$ and $\epsilon_{\text{network}} = 95\%$, calculated only for the red lightpath. In this subsection, the OSNR obtained with the ISRS GN models considers a null dispersion slope. In contrast to the closed-form ISRS GN-model, the asymptotic GN-model does not take into account the influence of the dispersion slope on the NLI prediction. Therefore, by considering a null dispersion slope, the comparison between the models is more fair. The remaining system parameters are the ones presented in Table 2.

In Fig. 8(a), since there is no considerable SRS power transfer for launch powers below 0 dBm, the difference between the OSNRs obtained is below 0.3 dB for all the GN models. For the optimum launch power of 0 dBm, in Fig. 8(b), the maximum discrepancy between the asymptotic GN-model and incoherent and coherent ISRS GN models increases to about 0.4 dB and 0.7 dB, respectively, due to the enhancement of the SRS effect. In Fig. 8(c), the considered CUTs power surpasses the optimal power of 0 dBm, and due to SRS, a much sharper tilt in the OSNR can be observed in the ISRS GN-model results. The maximum average power transfer rises, respectively, from 6 dB to 11.9 dB, for the 50 GHz channel spacing, and from 3 dB to 5.9 dB for the 100 GHz spacing, in relation to the 0 dBm launch power. Consequently, the maximum OSNR difference between the asymptotic GN-model and coherent and incoherent ISRS GN models increases, respectively, to about 3 dB and 2.4 dB. Fig. 8 shows that the OSNR variation along the CUTs frequency given by the asymptotic GN-model does not predict the OSNR tilt, leading to higher discrepancies for more pronounced OSNR tilts. Fig. 8 shows also that the difference between the OSNRs estimated by the coherent and incoherent ISRS GN models increases for higher CUT powers, reaching its highest value of around 0.7 dB and 0.8 dB for $\Delta f = 50$ GHz and $\Delta f = 100$ GHz, respectively.

As a main conclusion, the results presented in this subsection show that the asymptotic GN-model can provide reasonably accurate OSNR predictions in C+L band optical networks at optimum launch power, but can lead to up to 3 dB differences in the OSNR, when the SRS is significant.

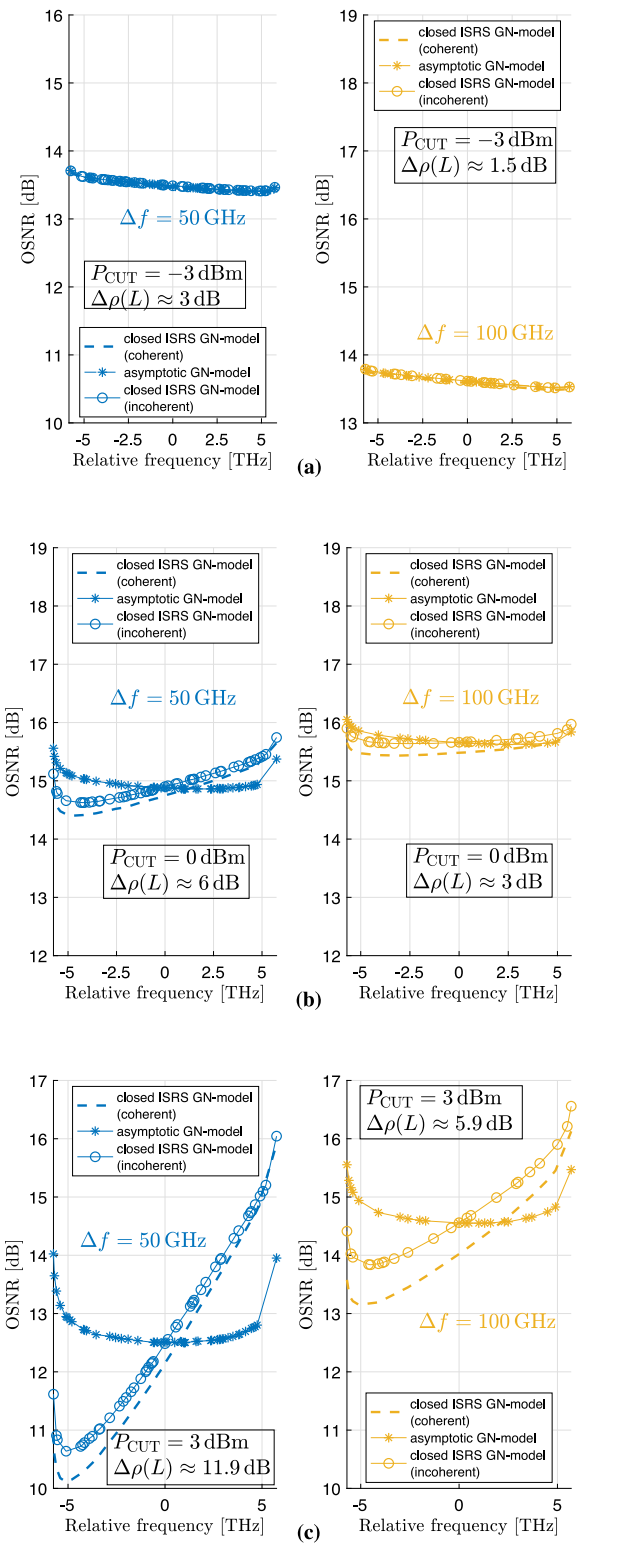

Fig. 8. OSNR as a function of the CUTs frequencies, for $\epsilon_{\text{occupancy}} = 100\%$, $\epsilon_{\text{network}} = 95\%$, $N_{CUT} = 20\% \cdot N_{ch}$, $S_r = 0$ ps/nm^2/km and the launch powers of (a) −3 dBm, (b) 0 dBm and (c) 3 dBm. Channel spacings $\Delta f = 50$ GHz and $\Delta f = 100$ GHz are used. Circles: closed ISRS GN-model (incoherent). Dashed lines: closed ISRS GN-model (coherent). Asterisks: asymptotic GN-model. Points: $\Delta\rho(L)$.

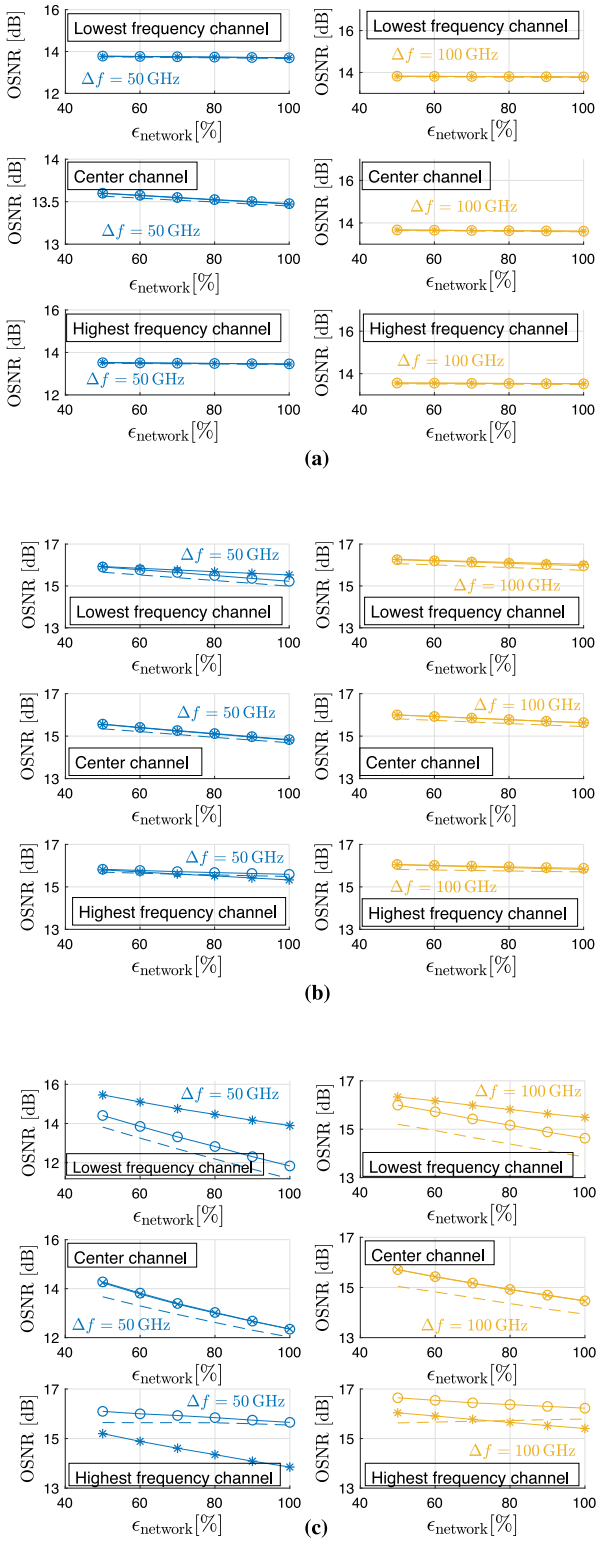

Fig. 9. OSNR for the red lightpath as a function of the network utilization, for $\epsilon_{\text{occupancy}} = 100\%$ and (a) $P_{CUT} = -3$ dBm, (b) $P_{CUT} = 0$ dBm and (c) $P_{CUT} = 3$ dBm. Only results for the lowest (−5.7 THz), center and highest (5.7 THz) frequency channels are presented, for $\Delta f = 50$ GHz and 100 GHz. Lines with circles: closed-form ISRS GN-model (incoherent). Dashed lines: closed-form ISRS GN-model (coherent). Lines with asterisks: asymptotic GN-model.

4.3. OSNR for different network utilizations

Lastly, it is important to analyze how the network utilization impacts the performance of the GN models when the WDM signal covers the full C+L band, i.e., $\epsilon_{\text{occupancy}} = 100\%$. The OSNR as a function of $\epsilon_{\text{network}}$ is represented in Fig. 9(a) for $P_{\text{CUT}} = -3$ dBm, in Fig. 9(b) for $P_{\text{CUT}} = 0$ dBm and in Fig. 9(c) for $P_{\text{CUT}} = 3$ dBm. The CUTs are chosen in the same way as described for Fig. 7.

The good agreement between the models predictions for $P_{\text{CUT}} = -3$ dBm is due to the lower power transfer of only 3.1 dB, which occurs when $\epsilon_{\text{network}} = 100\%$ and $\Delta f = 50$ GHz. For $P_{\text{CUT}} = 0$ dBm, the overall power transfer increases, leading to higher differences between the OSNR estimates as the network utilization increases, as can be observed in Fig. 9(b). The OSNR differences using the incoherent ISRS GN-model and the asymptotic GN-model reach about 0.3 dB in the edge channels when $\epsilon_{\text{network}} = 100\%$ and $\Delta\rho(L) \approx 6.2$ dB. For the coherent ISRS GN-model and for $\Delta f = 50$ GHz, the OSNR deviation in the lowest frequency channel relative to the asymptotic GN-model is about 0.3 dB and 0.5 dB for $\epsilon_{\text{network}} = 50\%$ and $\epsilon_{\text{network}} = 100\%$, respectively. For $\Delta f = 100$ GHz, this discrepancy is always below 0.3 dB. For the highest frequency channel, the OSNR estimates are very similar to the estimates of the asymptotic GN-model for all $\epsilon_{\text{network}}$ considered.

For $P_{\text{CUT}} = 3$ dBm, the OSNR predictions from the GN models follow a similar behavior as with $P_{\text{CUT}} = 0$ dBm, but due to the higher power transfer, the OSNR differences between the models for the edge channels become larger, for all network utilizations considered. For instance, for the lowest frequency channel with $\Delta f = 50$ GHz, the asymptotic GN-model overestimates the OSNR at least by about 1 dB and 2 dB for $\epsilon_{\text{network}} = 50\%$ and $\epsilon_{\text{network}} = 100\%$, respectively. For $\Delta f = 100$ GHz, the maximum OSNR difference is about 1.6 dB for the lowest frequency channel.

5. Conclusion

In this work, we studied the impact of the network utilization and several other network parameters on the QoT of multiband C+L networks using the closed-form ISRS GN-model. It was concluded that a variation in the network utilization from 20% to 100% leads to a power transfer increase of about 5.1 dB and 16.4 dB for the launch powers of 0 dBm and 5 dBm, respectively. With unequal CUTs spacing along the spectrum, we show that, due to the dynamic traffic behavior, the normalized NLI power can oscillate 2 dB along the WDM channels spectrum. We also demonstrated that, for the optimum launch power, the maximum OSNR variation along the channel frequencies is only about 0.7 dB.

Additionally, by comparing the performances of the asymptotic and ISRS GN models in optimum OSNR conditions and for full C+L band occupancy, the maximum OSNR difference using the asymptotic GN-model is only 0.7 dB compared to the optimum OSNR obtained with the ISRS GN-model. Hence, we have shown that, at optimum launch power and for applications that do not have high accuracy requirements, the asymptotic GN-model can represent a viable alternative to estimate the NLI in C+L band transmissions systems for average power transfers below 6 dB. It is expected that most optical networks are working near this low nonlinear effects regime [8]. However, for higher launch powers that lead to higher SRS power transfers, the use of the asymptotic GN-model is not recommended, because the OSNR discrepancies can increase up to 3 dB.

CRediT authorship contribution statement

Pedro Venda: Software, Validation, Formal analysis, Investigation, Data curation, Writing – original draft, Writing – review & editing, Visualization. **João Rebola:** Conceptualization, Methodology, Validation, Formal analysis, Investigation, Resources, Data curation, Writing – review & editing, Visualization, Supervision, Project administration. **Luís Cancela:** Conceptualization, Methodology, Validation, Formal analysis, Investigation, Resources, Data curation, Writing – review & editing, Visualization, Supervision, Project administration.

Declaration of competing interest

The authors declare that they have no known competing financial interests or personal relationships that could have appeared to influence the work reported in this paper.

Data availability

The authors are unable or have chosen not to specify which data has been used.

Acknowledgment

This research received no external funding.

References

[1] N. Sambo, et al., Provisioning in multi-band optical networks, J. Lightw. Technol. 38 (9) (2020) 2598–2605.
[2] M. Mehrabi, H. Beyranvand, M.J. Emadi, Multi-band elastic optical networks: Inter-channel stimulated Raman scattering-aware routing, modulation level and spectrum assignment, J. Lightw. Technol. 39 (11) (2021) 3360–3370.
[3] D. Uzunidis, E. Kosmatos, C. Matrakidis, A. Stavdas, A. Lord, Strategies for upgrading an operator's backbone network beyond the C-band: towards multi-band optical networks, IEEE Photonics J. 13 (2) (2021) 7200118.
[4] P.J. Winzer, D.T. Neilson, From scaling disparities to integrated parallelism: a decathlon for a decade, J. Lightw. Technol. 35 (5) (2017) 1099–1115.
[5] Cisco annual internet report (2018–2023), Cisco Systems, 2020, Available online: https://www.cisco.com/c/en/us/solutions/collateral/executive-perspectives/annual-internet-report/white-paper-c11-741490.html.
[6] B. Correia, R. Sadeghi, E. Virgillito, A. Napoli, N. Costa, J. Pedro, V. Curri, Power control strategies and network performance assessment for C+L+S multiband optical transport, J. Opt. Commun. Netw. 13 (7) (2021) 147–157.
[7] M. Cantono, R. Schmogrow, M. Newland, V. Vusirikala, T. Hofmeister, Opportunities and challenges of C+L transmission systems, J. Lightw. Technol. 38 (5) (2020) 1050–1060.
[8] D. Semrau, R.I. Killey, P. Bayvel, The Gaussian noise model in the presence of inter-channel stimulated Raman scattering, J. Lightw. Technol. 36 (14) (2018) 3046–3055, arXiv:1801.02460.
[9] M. Cantono, J.L. Auge, V. Curri, Modelling the impact of SRS on NLI generation in commercial equipment: an experimental investigation, in: Proc. Opt. Fiber Commun. Conf. Expo., San Diego, CA, USA, 2018, paper M1D.2.
[10] A. Ferrari, et al., GNPy: an open source application for physical layer aware open optical networks, J. Opt. Commun. Netw. 12 (6) (2020) C31–C40.
[11] M. Cantono, D. Pilori, A. Ferrari, V. Curri, Introducing the generalized GN-model for nonlinear interference generation including space/frequency variations of loss/gain, 2017, arXiv preprint arXiv:1710.02225.
[12] A. Ferrari, et al., Experimental validation of an open source quality of transmission estimator for open optical networks, in: Proc. Opt. Fiber Commun. Conf. Expo., IEEE, San Diego, CA, USA, 2020, pp. 1–3, paper W3C.2.
[13] D. Semrau, R.I. Killey, P. Bayvel, A closed-form approximation of the Gaussian noise model in the presence of inter-channel stimulated Raman scattering, J. Lightw. Technol. 37 (9) (2019) 1924–1936.
[14] A. Mitra, et al., Effect of reduced link margins on c+l band elastic optical networks, J. Opt. Commun. Netw. 11 (10) (2019) C86–C93.
[15] A. Mitra, et al., Effect of channel launch power on fill margin in C+L band elastic optical networks, J. Lightw. Technol. 38 (5) (2020) 1032–1040.
[16] T. Ahmed, A. Mitra, S. Rahman, M. Tornatore, A. Lord, B. Mukherjee, C+L-band upgrade strategies to sustain traffic growth in optical backbone networks, J. Opt. Commun. Netw. 13 (7) (2021) 193–203.
[17] P. Johannisson, E. Agrell, Modeling of nonlinear signal distortion in fiber-optic networks, J. Lightw. Technol. 32 (23) (2014) 4544–4552.
[18] J. Pedro, Designing transparent flexible-grid optical networks for maximum spectral efficiency, IEEE/OSA J. Opt. Commun. Netw. 9 (4) (2017) C35–C44.
[19] D. Sequeira, L. Cancela, J. Rebola, CDC ROADM design tradeoffs due to physical layer impairments in optical networks, Opt. Fiber Technol., Mater. Devices Syst. 62 (2021) 102461.
[20] D.J. Ives, A. Lord, P. Wright, S.J. Savory, Quantifying the impact of non-linear impairments on blocking load in elastic optical networks, in: Proc. Opt. Fiber Commun. Conf., 2014, paper Th1E.6.
[21] A. Ferrari, et al., Assessment on the achievable throughput of multi-band ITU-T G.652.D fiber transmission systems, J. Lightw. Technol. 38 (16) (2020) 4279–4291.
[22] P. Poggiolini, The GN model of non-linear propagation in uncompensated coherent optical systems, J. Lightw. Technol. 30 (24) (2012) 3857–3879.